

PARAMETRIC STUDY ON DENSITY STRATIFICATION EROSION CAUSED BY A HORIZONTAL STEAM JET INTERACTING WITH A VERTICAL PLATE OBSTRUCTION

S. Paranjape, R. Kapulla, G. Mignot and D. Paladino

Paul Scherrer Institut, Switzerland

Villigen-PSI, CH-5210

Sidharth.paranjape@psi.ch; ralf.kapulla@psi.ch; guillaume.mignot@psi.ch;
domenico.paladino@psi.ch

ABSTRACT

During postulated severe accident scenarios in nuclear power plants, a hydrogen-rich layer might form at the top of the reactor containment. Various flow patterns resulting from the release of steam from the primary circuit might break the layer and redistribute hydrogen in the containment. The prediction of the gas transport during the accident requires detailed modeling of the processes involved. Advanced lumped parameter codes or computational fluid dynamics codes are used for this purpose. These codes need to be validated against experimental data obtained in large scale experimental facilities, where scale distortions are reduced. In order to obtain the required data with high spatial and temporal resolution, experiments were carried out in the PANDA facility in Switzerland as a part of OECD/HYMERES (HYdrogen Mitigation Experiments for Reactor Safety) project. The present experiments address the breakup of a layer rich in helium (used as simulant for hydrogen), under steam environment and its redistribution in two interconnected vessels (total volume of 183.3 m³) under the action of a diffused flow resulting from the interaction of a horizontal steam jet with a vertical plate obstruction. The influence of the distance between the jet exit and the obstruction on the flow pattern was investigated. Spatial and temporal distribution of the gas concentration, the temperature and local gas velocity field were measured. It was found that a small change in the geometric configuration lead to a large change in the flow pattern. Reducing the jet-obstruction distance slowed down the helium-layer erosion process significantly. Additionally, the creation of a concentration stratification in the adjacent vessel connected by an interconnecting pipe was observed.

KEYWORDS

Severe accident, Hydrogen mitigation, diffused jet, stratification erosion

1 INTRODUCTION

Hydrogen generated during a postulated severe accident in nuclear light water reactors (LWR) with core degradation is a major safety issue, because explosive mixtures could form in the containment or in the containment building. Therefore, the nuclear research community, since many years, has identified the composition of the containment atmosphere (hydrogen, steam, air) and the mixing and stratification phenomena associated with the distribution of gases as high-ranking issue for nuclear power plant safety which requires further research (OECD/NEA/WGAMA [1], SARNET/SARP [2]).

Analysis of thermal-hydraulic processes occurring in a nuclear power plant containment building under severe accident conditions is complicated. The complexity stems from: i) the geometry of the various components inside the containment building, ii) sequential or simultaneous performance of active (e.g. sprays, coolers, etc.) or passive safety systems (e.g. PARs, rupture foils, passive condensers, etc.), and iii) different types of physical phenomena occurring during the transient, e.g. the presence of jets and plumes (with positive or negative buoyancy), mixing and stratification, transport induced by density or pressure differences, condensation induced by the proximity of a cold wall or the activation of safety systems, re-evaporation phenomena, etc. Owing to these complexities, the advanced LP and CFD codes used for analyzing LWR behavior during postulated design and beyond-design-basis accidents need extensive validation against experimental data collected under close-to-prototypic conditions [3,4]. In this respect, experiments using large scale facilities are preferable due to reduced geometrical scale distortion. The large-scale facilities PANDA and MISTRA have been used in the last years in several international projects (e.g. OECD/SETH and SETH-2 [5], Euroatom-Rosatom ERCOSAM-SAMARA [6]) devoted to the issue of hydrogen distribution.

The on-going project HYMERES (HYdrogen Mitigation Experiments for Reactor Safety) is an OECD/NEA project with PSI and CEA Operating Agents, performing experiments respectively in PANDA and MISTRA facilities, and is supported by Organizations from 13 Countries [7]. The main objective of the HYMERES Project is to improve the understanding of the hydrogen risk phenomenology in containment in order to enhance its modelling in support of safety assessment that will be performed for current and new nuclear power plants.

This paper presents results of two tests, namely, HP1_2 and HP1_3, which belong to a series of 8 tests addressing gas mixture stratification break-up by “diffuse flow” resulting from the interaction of a jet/plume with flow obstructions. HP1_2 and HP1_3 consider the breakup of a layer rich in helium (simulating hydrogen), with composition of 25% molar helium, 75% molar steam, under steam environment, 100% steam at 108°C, 1.3 bar, and its redistribution in two interconnected vessels under the action of a diffused flow resulting from the interaction of a horizontal steam jet at 40g/s, 150°C with a vertical plate obstruction. The influence of the distance between the jet exit and the obstruction on the flow pattern was investigated, by varying the distance between the two tests. Spatial and temporal distribution of the gas concentration was measured using sampling capillaries connected to a mass-spectrometer, while that of the gas temperature was measured using thermocouples. The local gas velocity field was measured using Particle Image Velocimetry (PIV) at selected temporal windows for particular field of views, which highlighted the flow structures near the helium layer mixing zone.

Following this introduction, a description of the experimental facility is given along with experimental procedure. Measured initial and boundary conditions are presented. Experimental results are discussed, where the observations from the two tests are compared. Finally, the main findings from the experiments are summarized. Scales are not shown in some of the plots, because the data is not publicly available owing to the terms of HYMERES project agreements. However, the data will be accessible in public domain in the year 2020.

2 EXPERIMENT

2.1 Experimental Facility

The PANDA facility is a large scale, multi-compartmental thermal hydraulic facility suited for investigations related to the safety of current and advanced LWRs [8]. The experiments were carried out in a large double compartment with 183.3 m³ total volume consisting of the two identical drywell vessels (Vessel 1 and Vessel 2) having a height of 8 m and a diameter of 4 m each. Both vessels are marked red in the upper part of Fig. 1(a). Vessel 1 and 2 are connected by a large interconnecting pipe (IP) with a

diameter of 1 m. To minimize heat losses, the entire facility is thermally insulated with 20 cm thick rock-wool mat. The RPV was used as a steam source to inject superheated steam in to Vessel 1.

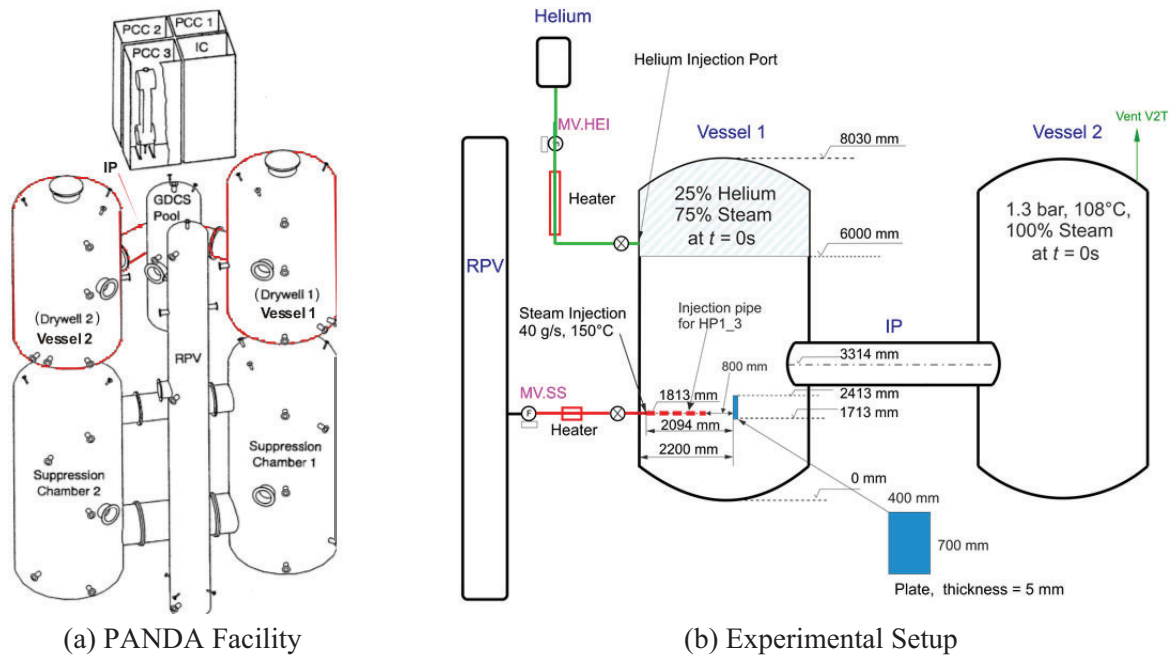


Figure 1. PANDA Experimental Facility.

A schematic diagram of the experimental setup used for two experiments presented in this paper is shown in Fig. 1(b). For the formation of the helium layer at the top of Vessel1, helium is injected through a pipe located at the elevation of 6 m from the bottom of Vessel 1. The helium flow rate is measured by a helium flow meter in order to inject specified amount of Helium in to Vessel 1. A heater is used to increase the temperature of helium. To create a horizontal steam jet, a port having 153 mm inner diameter is provided in Vessel 1 at the elevation of 1813 mm from the bottom of Vessel 1. A vertical flow obstruction is installed in Vessel 1 in the form of a rectangular plate with a width of 400 mm and a height of 700 mm. The bottom of the plate is located at the elevation of 1713 mm. The distance between the wall of Vessel1, at the location of the steam injection port and the plate is 2200 mm. This arrangement of horizontal steam jet and the obstruction is used for the test HP1_2. For the second test, HP1_3, a double-walled pipe with an internal diameter of 153 mm is connected to this port, extending into Vessel 1 by 1400 mm from the inside wall of the vessel. Thus, the distance between the plate and the exit of the steam injection pipe is reduced to 800 mm. In order to reduce heat loss from the injection pipe, vacuum is created in the gap of the walls of the pipe. The plate is oriented in such a way that the normal to the plate surface is parallel to the direction of the steam injection. The plate is placed symmetrically with respect to the axis of the injection pipe in horizontal direction, perpendicular to the plane of Fig. 1(b). To maintain a constant pressure in the vessels, a vent to the atmosphere is provided in Vessel 2, shown as “Vent V2T” in Fig 1(b). To control the vessel pressure, a valve is installed at the vent. The opening of the valve is adjusted according to the pressure reading from the vessels. The nominal initial and boundary conditions are also depicted in Fig. 1(b).

2.2 Instrumentation

The three main measurement systems used in the PANDA Vessels 1 and 2 are (1) temperature sensors, (2) concentration measurement devices, and (3) Particle Image Velocimetry (PIV) system for 2D velocity

measurement. In addition, absolute and differential pressures, flow rates, heating power, water level, and automatic valve status were recorded.

The sensor grid for the temperature and concentration measurements in Vessel 1 and in Vessel 2 has a high spatial resolution well suited for the envisaged code validation purposes. Up to 380 K-type thermocouples (TCs) were used for measuring fluid as well as inside and outside wall temperatures of Vessel 1, Vessel 2, and the IP. Through calibration of these thermocouples, an accuracy of 0.7°C was assessed. Temperature sensors were installed in the vessels at different heights identified as level A (near the top of the vessels) to level T (near the bottom of the vessel) and at different radial distances from the vessel axis.

The gas concentration was measured by two mass spectrometers (MS). Gas was continuously sampled through capillaries located adjacent to selected thermocouples such that gas concentration and temperature measurements were available at almost the same spatial location. For steam/helium mixtures, an absolute error on the measured steam/helium molar fraction of $\pm 1.5\%$ was assessed.

Particle Image Velocimetry was used for the measurement of 2-D velocity fields. After calibration of the images, an effective spatial resolution of $10.3 \times 10.3 \text{ mm}^2$ for the velocity field is obtained. The PIV light sheet was generated in the 135° - 315° plane, which is inclined with respect to the IP-plane (125° - 305°), Fig. 2, top view, right part. The measurements were taken at three different field-of-views (FOVs) to follow the erosion front progression of the helium layer, depicted as PosA, PosB and PosC in Fig. 2. For the calculation of statistical quantities 1024 image pairs consisting of statistically independent samples were averaged which results in an overall averaging time of 204.8 s. An average value for the mean axial velocity would typically be of magnitude $v \approx 0.1 \text{ m/s}$, with a standard deviation of around $v_{\text{rms}} \approx 0.08 \text{ m/s}$. Thus, the two-sided uncertainty, with 95% confidence level, is estimated at $\epsilon(v) = \pm 0.005 \text{ m/s}$ for the mean vertical velocity. Analogous estimates apply also for the lateral velocities ($u \approx 0.2 \text{ m/s}$) and result in $\epsilon(u) = \pm 0.0061 \text{ m/s}$. The details of measurement systems used in PANDA are discussed elsewhere [11].

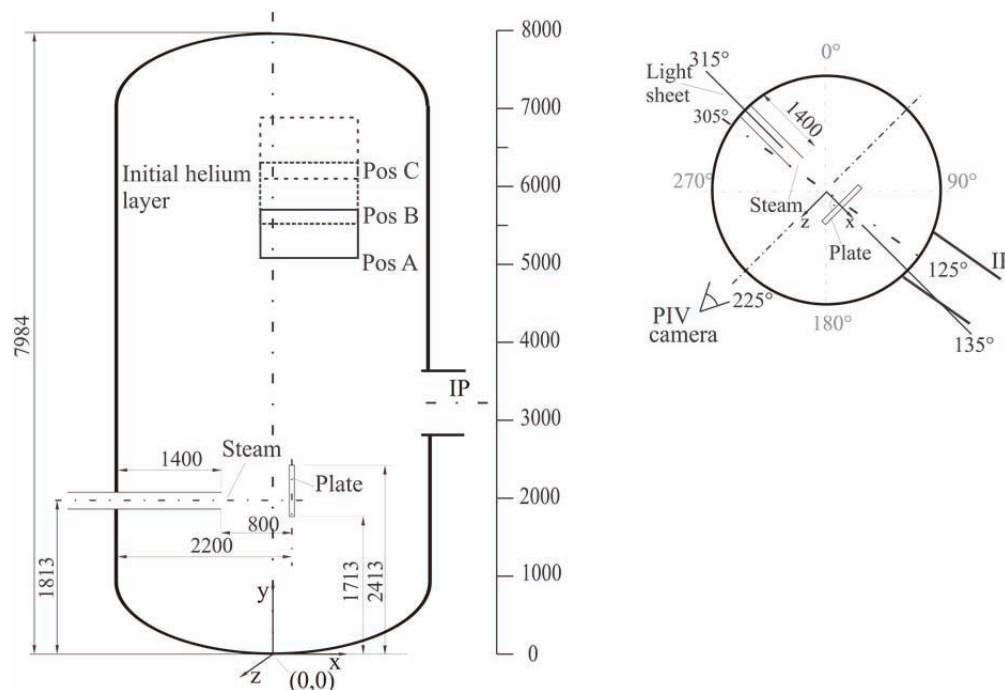


Figure 2. Schema of PIV Measurement Setup

2.3 Test Procedure and Initial and Boundary Conditions

The facility preconditioning started with the creation of a 100% steam atmosphere in both of the PANDA vessels. This was achieved by injecting steam at 108°C into the vessels, while purging the air from vent lines. Condensed water was drained from the bottom of the vessels. Pressure of 1.3 bar (nominal) was maintained in the vessels. The procedure was continued till vessel walls reached the temperature corresponding to the saturation temperature for 1.3 bar. After reaching these conditions, helium was injected in Vessel 1 at a flow rate of 4g/s for 210 s to create a nominal 25% helium layer above the height of 6 m. A short relaxation phase of 360 s was started after the injection of helium, during which gas concentrations in the Helium-rich layer were recorded with the Mass Spectrometer. The measurements during the relaxation phase represent the initial conditions for the test.

The initial conditions for the test are measured during the relaxation phase, before the start of the main test phase ($t = 0$ s), over a period of -340s to -40s. The measured gas concentration and calculated densities for Vessel 1 at the initial condition for the two tests are presented in Fig 3(a,b).

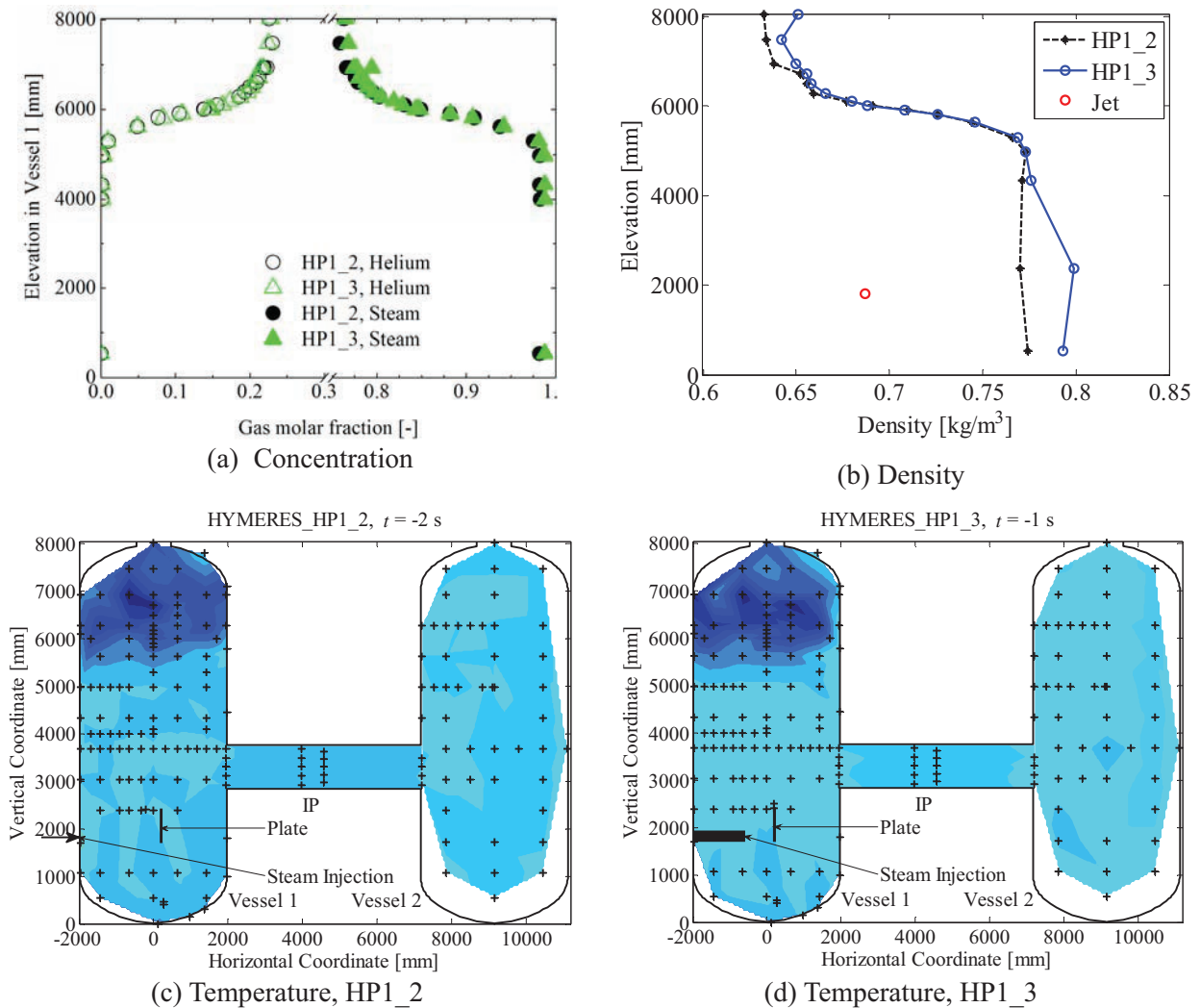


Figure 3. Initial Conditions

The helium layer is above 6000 mm, with a diffused interface towards the steam environment below the layer. The density distribution shows a smooth transition from higher density in the lower part to lower density above 6000 mm. The density of injected steam jet lies between the ambient fluid density and the helium layer density. Thus, the jet is initially buoyant with respect to the ambient, but negatively buoyant (heavier) with respect to the helium layer. The temperature distribution at initial condition is uniform below the helium layer, Fig. 3(c,d). Since the injected helium is at a lower temperature than the steam in the vessels by about 4°C, the extent of the helium layer is visible in Fig. 3(c,d).

The main test phase was started after the relaxation phase, by injection of superheated steam at 150°C, with a flow rate of 40 g/s. To maintain the constant pressure of 1.3 bar (nominal) in the vessels, gases were continuously vented to the atmosphere through a vent line located in Vessel 2. The steam injection was continued till the initial helium layer was completely broken.

3 RESULTS

The horizontal steam jet injected into Vessel 1 generates a diffused flow in the vertical direction after interacting with the vertical plate obstruction. The diffused flow impinges on the lower density helium layer, entraining the gas from the layer and hence leading to erosion of the helium layer. In addition, the steam injection also induces flow between the two vessels through the interconnecting pipe, redistributing the helium in the vessels. The details of these processes are discussed in this section with reference to the evolution of the measured temperature, the local two-dimensional velocity, the gas species concentration and the derived quantity, gas mixture density.

The overall gas circulation in the vessels can be inferred from the temperature contour plots obtained at various time instances, Fig. 4(a,c,e) for HP1_2 and Fig. 5(a,c,e) for HP1_3. Both tests exhibit higher temperature near the top of the plate obstruction (~2400 mm elevation) compared to the locations at the same elevation, radially located between the jet and the plate. This suggests that the horizontal jet impinges on the plate. Thus, the plate plays a role in re-distribution of the flow from the jet. However, since the jet-plate distance is different for the two tests, the flow structure above the level of the plate is significantly different. Significant thermal asymmetry with respect to Vessel 1 axis is observed in HP1_2 compared to that in HP1_3. HP1_2 exhibits higher temperatures on the opposite side of the jet, indicating that the flow from the jet interacts to a lesser extent with the plate compared to that in HP1_3 and reaches near the wall opposite to that of the jet. The temperature contour maps (Fig. 4(a,c,e)) suggest a formation of a large scale vortex with flow rotating counter clockwise. An inclined helium layer interface is observed during the early part of the layer erosion process for HP1_2, Fig. 4(a). On the other hand, the thermal symmetry in HP1_3 test indicates diffused flow mostly in the vertical direction. The impact of the obstruction plate is greater on the deflection of the jet flow, in case of HP1_3. The temperature contour maps for both of the tests show thermal stratification in the interconnecting pipe, and slightly higher temperature in the upper part of Vessel 2, on the side of the IP. This indicates flow of gases from Vessel 1 to Vessel 2 through the upper part of IP, forming a plume in Vessel 2.

The two dimensional time averaged velocity fields at time instances corresponding to the temperature maps are presented in Fig. 4(b,d,f) for HP1_2 and in Fig. 5(b,d,f) for HP1_3. In the velocity fields, the vectors are colored according to the two-dimensional velocity magnitude. For HP1_2 test, the stream lines indicate the presence of a large scale vortex positioned asymmetrically with respect to the axis of Vessel 1. The center of curvature of the average velocity stream lines appear to be near the radial location of +600 mm. The average velocity stream lines show the existence of a mixing layer, which is inclined with respect to horizontal direction by about 40°. In contrast, the stream lines are less asymmetric in case of HP1_3, Fig. 5(b,d). During the early part of HP1_3 ($t_c = 249s$), the plume resultant from the jet-plate interaction appears to be positioned on the positive x direction, though the center of curvature of the stream lines appears on the negative x direction, Fig. 5(b). However, the velocity field obtained later

in time, *i.e.*, at $t_c = 3226.4s$, shows an inclined mixing region, Fig. 5(e). Compared to HP1_2, the velocity magnitudes in HP1_3 are lower near the helium layer interface. In case of HP1_3, the rising plume is decelerated to a greater extent due to its interaction with the downward flowing fluid, compared to that in case of HP1_2, where the strong asymmetric position of the rising plume allows less interaction with the downward flowing fluid.

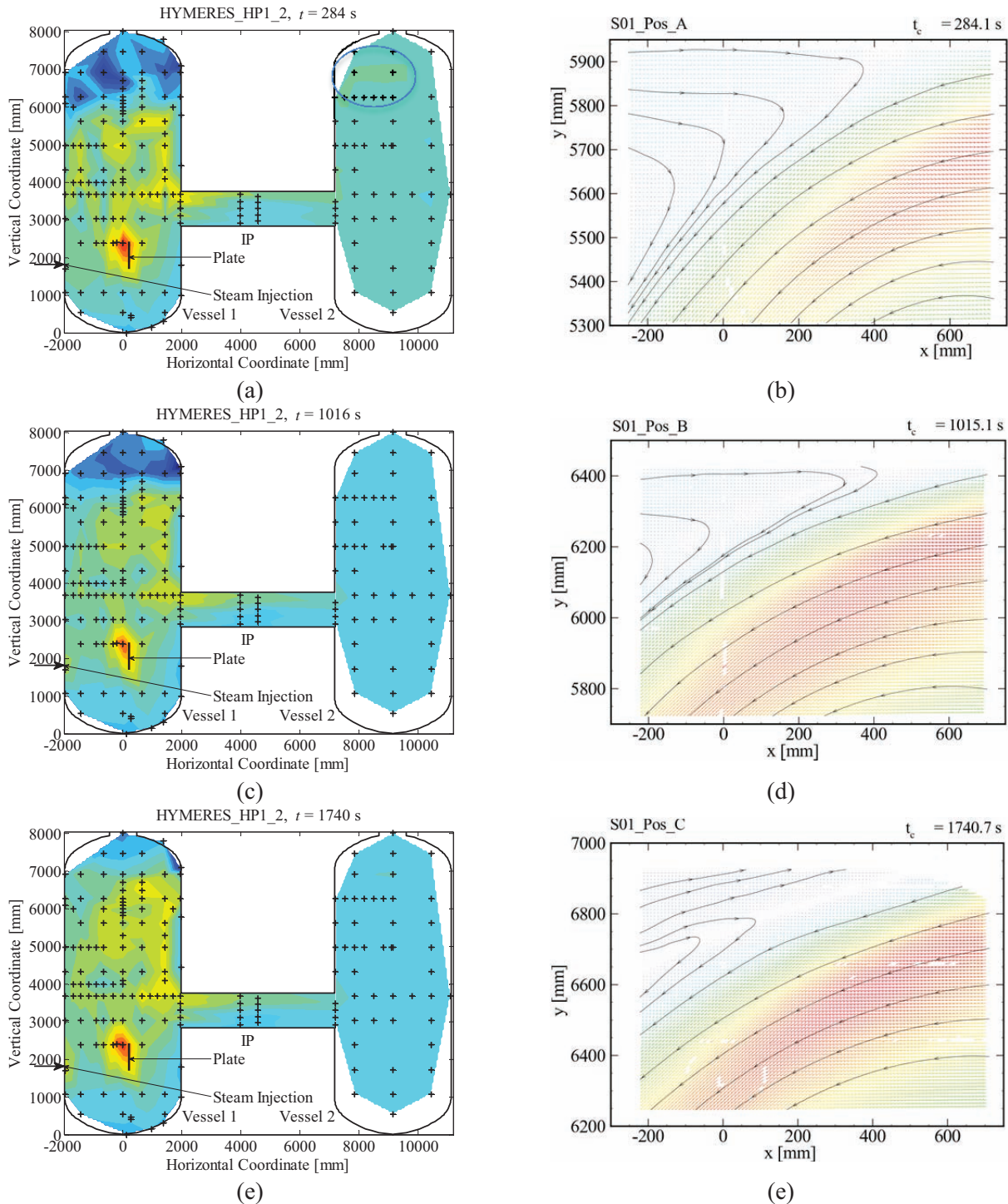


Figure 4. Temperature and Velocity Fields During HP1_2 Test.

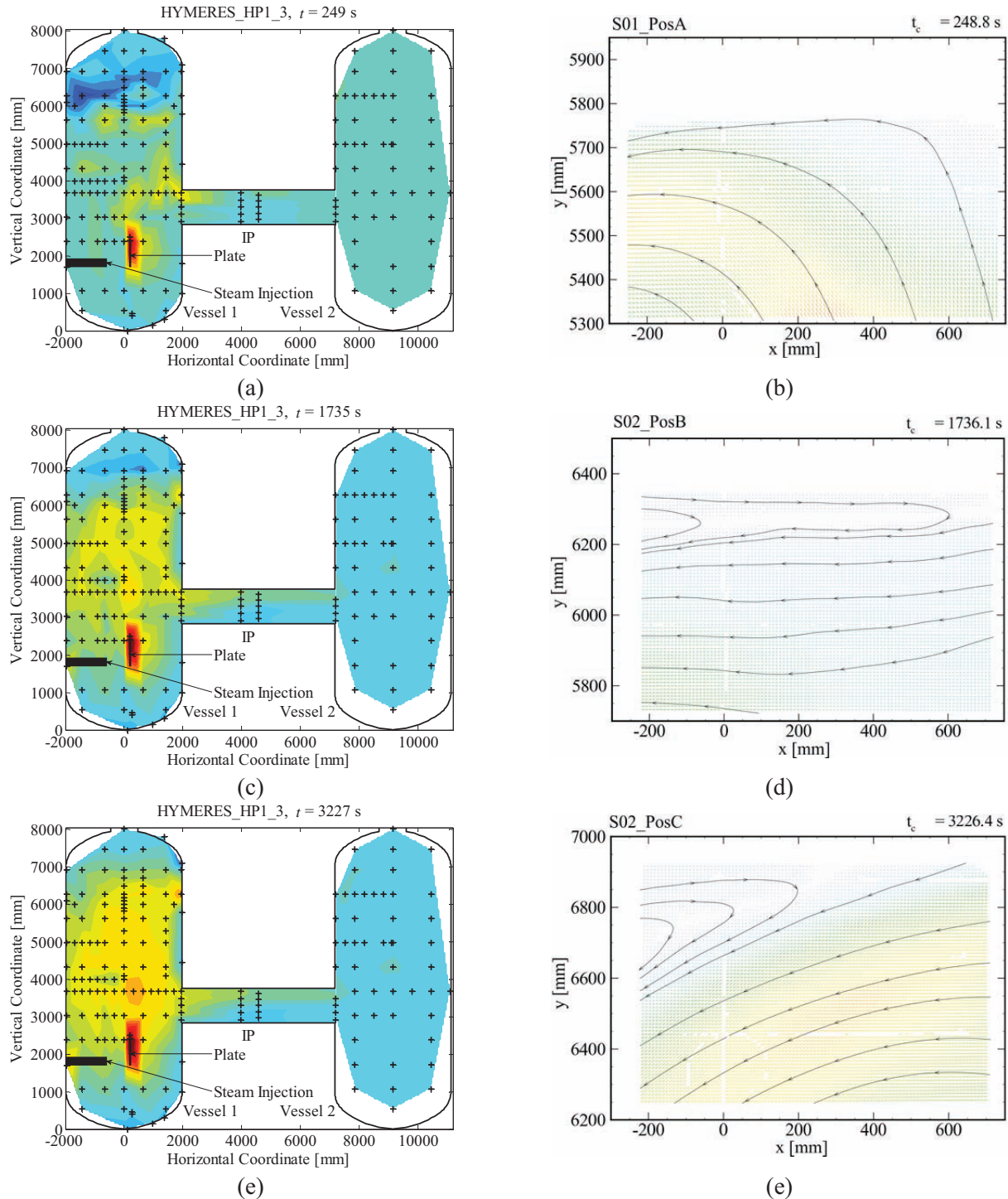


Figure 5. Temperature and Velocity Fields During HP1_3 Test.

The depletion of the helium layer and the transport of the gas species can be observed from the evolution of helium concentration at selected locations (Fig. 6) in the vessels measured using mass-spectrometers. As the plume generated from jet-plate interaction entrains helium from the layer, helium molar fraction reduces progressively with respect to the elevation in Vessel 1, Fig. 7(a,c). The duration for complete

erosion of the layer as indicated by sensor A_20 in both of the figures shows that erosion process is approximately *twice as fast* in case of HP1_2 compared to that of HP1_3.

During the experiments, the helium molar fraction in the layer decreases uniformly for all the sensors where the erosion front has not reached. This uniform depletion could be attributed to the gaseous diffusion. This uniform depletion rate is different for the two tests, indicated in Fig. 7(a,c), by slope of the best-fit lines drawn for the data points where the erosion front has not reached. It is interesting to note that the uniform depletion rate is *higher* in case of HP1_3, $\frac{dX_{He}}{dt} = -1.28 \times 10^{-5}/s$ than that for HP1_2, $\frac{dX_{He}}{dt} = -0.923 \times \frac{10^{-5}}{s}$, *i.e.*, by 37%. This shows that the location of plume impingement on the helium layer affects the overall diffusion rate. Both of these depletion rates are higher than the depletion rate for pure diffusion, $-0.884 \times 10^{-5}/s$, reported in a previous test as a part of SETH-2 project [9], where 25% helium-rich layer was created under the same conditions with no steam injection. Thus, the depletion rate for HP1_2 is enhanced by a factor of 1.044 over the pure diffusion case, while that for HP1_3 is enhanced by a factor of 1.45 over the pure diffusion case.

The asymmetry in the helium layer depletion in case of HP1_2 is clear from Fig. 7(b). The mole-fraction sensors located on the positive x direction, namely, B_22, C_26, F_27 show a reduction in helium molar concentration *earlier* than those located in the center and negative x direction. This time difference is larger for the sensor located lower elevation, F_27 than those at higher elevation C_26, B_22. These observations are consistent with the asymmetry observed by temperature maps and velocity fields. As expected, the helium layer depletion is symmetric for HP1_3, evident from Fig. 7(d). After complete depletion of the layer, marked by the concentration decay for sensor A_20, the helium concentration is uniform in Vessel 1 at helium molar fraction of approximately 0.02 in case of HP1_2 and approximately 0.01 for HP1_3. Since the helium layer depletion time for HP1_3 is about twice as that for HP1_2, number of moles of steam injected into the vessels is approximately double. Therefore, the asymptotic concentration of helium for HP1_3 is about half as that for HP1_2, given that all initial and boundary conditions are the same.

As helium layer is depleted, the entrained helium is transported to the adjacent Vessel 2 through IP. The earlier rise of helium concentration at locations A, D than at locations M, N in Vessel 2, shows that helium, is transported first to the upper part of Vessel 2 for both of the tests, Fig. 8(a,c). Concentration stratification is also observed in IP, Fig. 8(b,d). The fluid with higher temperature and higher concentration of helium, thus having lower density, flows through the upper part of IP. As the test progresses, helium concentration reaches uniformity for HP1_2, Fig. 8(b) while it becomes completely uniform and asymptotically constant for HP1_3, Fig. 8(d). The gas environment in Vessel 2 becomes stratified with negligible helium concentration at the bottom of Vessel 2, as evident from sensor T_20 in Fig. 8 (a,c). The inter-vessel transport has a qualitative similarity between the two tests. However, the asymptotic helium concentration above IP level is *twice* for HP1_2 as HP1_3. In both cases, the asymptotic helium concentration above IP in Vessel 2 is approximately same as that in entire Vessel 1 after complete depletion of the helium layer.

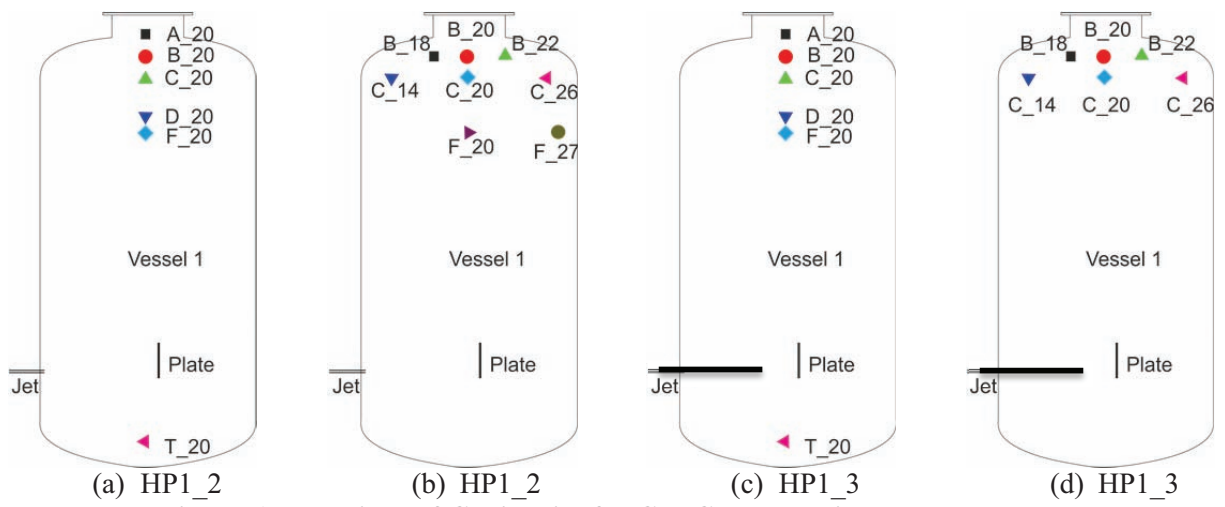


Figure 6. Locations of Capillaries for Gas Concentration Measurements

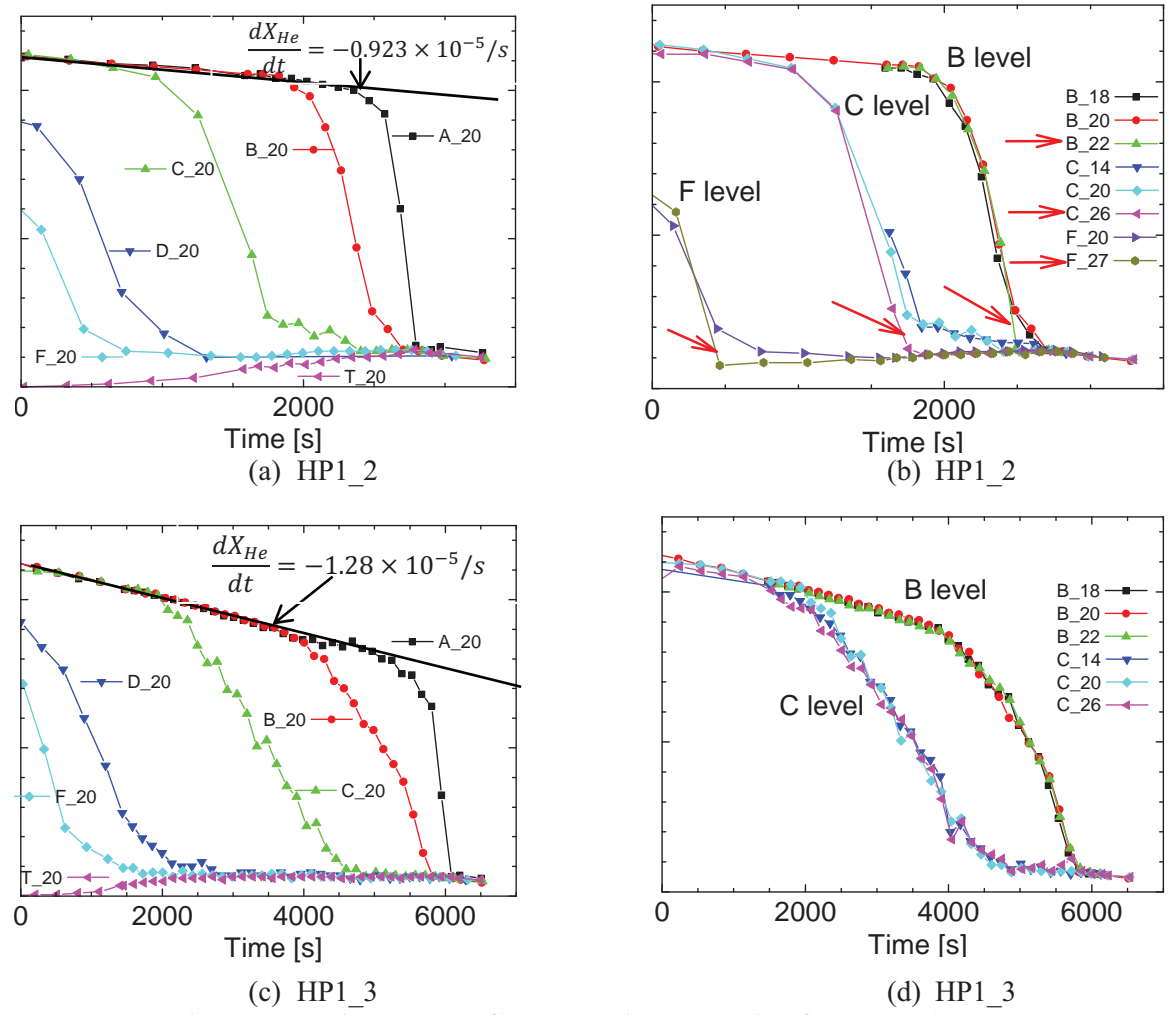


Figure 7. Helium Molar Concentration Evolution for Vessel 1

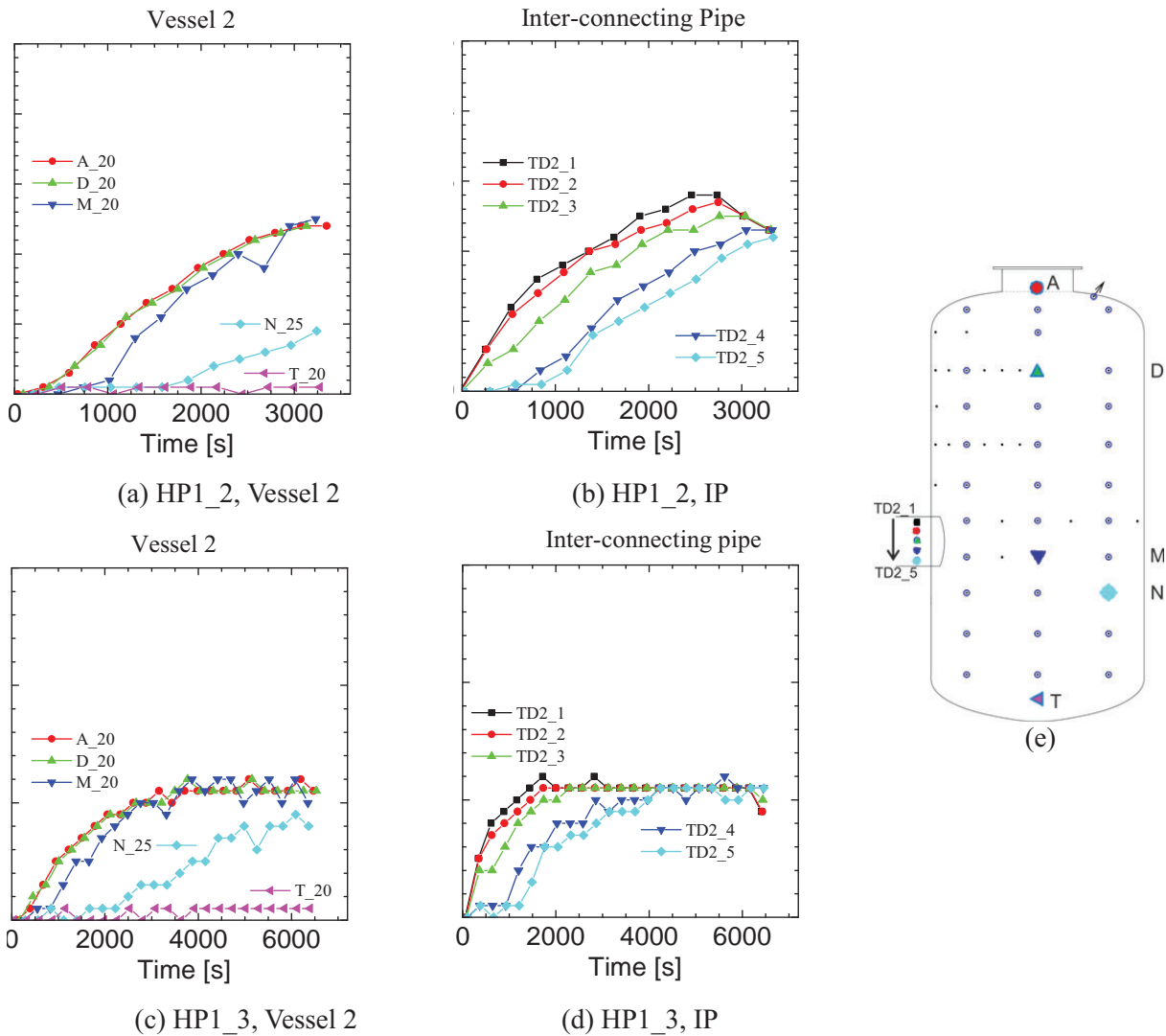


Figure 8. Helium Molar Concentration in Vessel 2 and Interconnecting Pipe

The helium concentration and the fluid temperature determine the fluid density and hence affect the momentum balance through the gravitational body force. Therefore it is useful to determine the vertical density distribution in the vessels. The evolution of the vertical density distribution in Vessel 1 is shown in Fig. 9. The legend shows the time instances (in seconds) at which the densities are calculated, “0” being the initial condition. The time instances are the same as those for the temperature maps and the velocity fields presented in the earlier part of this section. The density is lower above 6000 mm, where the helium layer is located. The density smoothly changes to a higher value for lower elevations, corresponding to the 100% steam conditions in the lower part of the vessel. In both of the tests, the density increases uniformly within the first 300 seconds. This is attributed to a slight rise in the pressure inside that vessel, by $\frac{\Delta p}{p_{initial}} = 0.04$, as steam is injected into the vessels. This is due to a delay involved in the regulating valve at the vent in Vessel 2 that controls the pressure inside the vessels. As the tests progress, the density transition layer is pushed upwards. The profiles are similar in both tests, but the time evolution is about twice as fast in HP1_2 as in HP1_3.

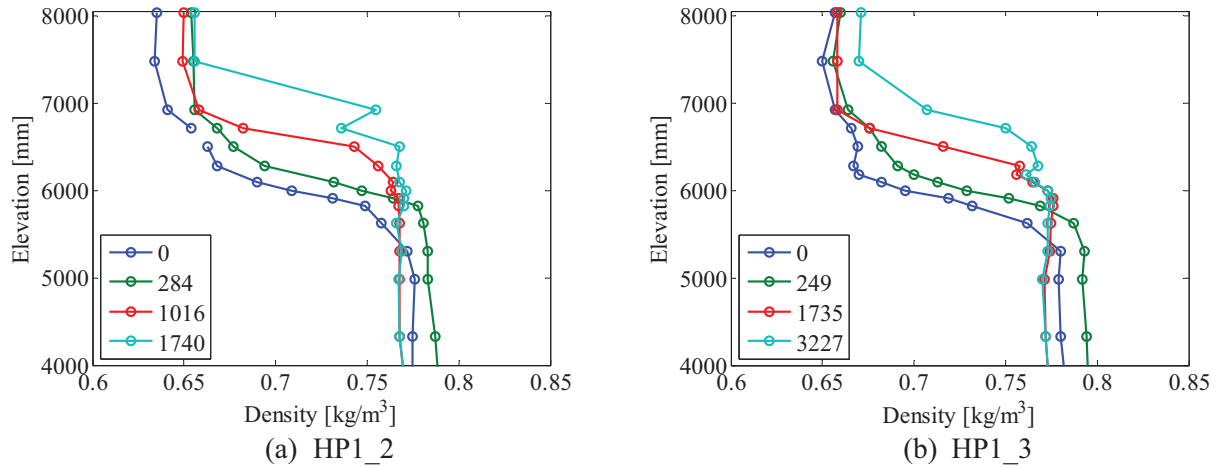


Figure 9. Evolution of Vertical Density Distribution

The quantitative comparison between the two tests is done by approximating the time evolution of the erosion front. The methodology used is similar to a previously published research on the subject as a part of OECD/NEA benchmark exercise [10]. The vertical density distribution is considered for this purpose, since it combines the concentration and temperature measurements. Since the density transition layer is not a sharp interface, a curve is fit to the density data as follows,

$$\rho(y) = a_1 + a_2 \left(1 - \left[1 + \exp \left\{ \left(y + a_4 \ln \left(2^{\frac{1}{a_5}} - 1 \right) \right) / a_3 \right\} \right]^{-a_5} \right), \quad (1)$$

where, ρ is the gas density at elevation y . The coefficients a_i are found through least squares curve fitting. The coefficient a_3 , is identified as the location of the center of the density transition layer. An example of the density distribution showing the extent of the density layer transition along with fitted curve is shown in Fig 10(a). The locations of the erosion front found by this method are plotted against time for both the tests, Fig. 10(b).

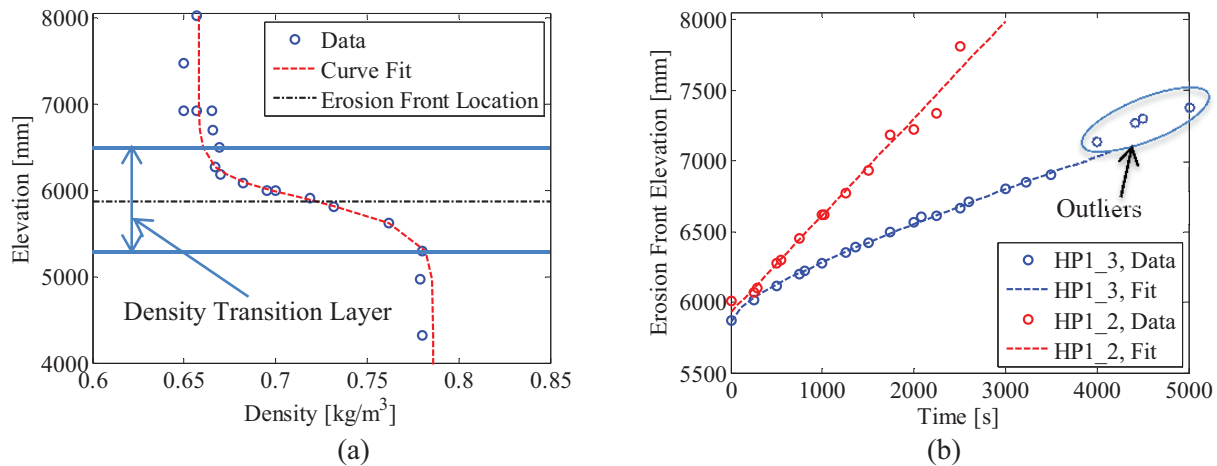


Figure 10. Evolution of Erosion Front

The erosion front not only moves slower for HP1_3, but also has a functional difference from that for HP1_2. HP1_2 shows the front propagation linear with time, while HP1_3 shows a combination of linear and square-root dependence on time. A linear fit to the erosion front motion for HP1_2 gives,

$$y_f(t) = v_f t + y_{f,0}, \quad (2)$$

where, $v_f = 0.686$ mm/s, and $y_{f,0} = 5928$ mm.

On the other hand, a linear plus square-root least-squares-error fit to erosion front motion for HP1_3 gives,

$$y_f(t) = v_{f,l} t + \sqrt{Dt} + y_{f,0}, \quad (3)$$

where, $v_{f,l} = 0.164$ mm/s, $D = 66.4$ mm²/s and $y_{f,0} = 5860$ mm. The fitted curves for both cases are shown in Fig. 10(b) by dotted lines. It should be noted that in the case of HP1_3, the data for $t > 4200$ s, marked as “outliers” in Fig. 10(b), is not considered. These points show a departure from the postulated functional dependence. It was observed that for $t > 4200$ s, the density transition layer reaches the curved part of the upper dome of Vessel 1, effecting a change in the dynamics of the erosion front motion, for which a simple mathematical expression may not be possible, but accessible only through detailed Computational Fluid Dynamics calculations. A slightly different functional dependence of helium layer erosion front motion has been reported for vertical buoyant jet impinging on a helium-rich layer under adiabatic air-helium environment in OECD-NEA-PSI benchmark exercise [10,11] as follows,

$$y^{-1} = a + bt^{0.5}, \quad (4)$$

Though this form of the equation gives a good approximation to the data, it has a singularity at large times, $t = (-\frac{a}{b})$, since coefficients a and b were found to be of opposite signs [10]. Nevertheless, Eq. (4) can be reduced to the form of Eq. (3) through binomial expansion to second order accuracy for the time range of interest. Therefore, functional form of Eq. (3) is preferred over Eq. (4) in the present analysis. The similarity of the erosion front motion for the test with shorter jet-obstruction distance, *i.e.*, HP1_3, with that of reported in previous research, in reference [10], suggests that it has a dynamics similar to that for a situation with a vertical jet.

4 CONCLUSIONS

Experiments were carried out to address the breakup of a layer rich in helium, used as simulant for hydrogen, under steam environment and its redistribution in two interconnected vessels of the PANDA facility, due to the action of a diffused flow resulting from the interaction of a horizontal buoyant steam jet with a vertical plate obstruction. The influence of the distance between the jet exit and the obstruction on the flow pattern was investigated through two tests, HP1_2 and HP1_3, in the frame of HYMERES project. The measured spatial and temporal distribution of the gas concentration, the gas temperature and the local gas velocity field revealed the flow structures and the process of helium layer erosion. It was found that a small change in the geometric configuration, *i.e.*, change in the jet-plate obstruction distance lead to a large change in the flow pattern. Reducing the jet-obstruction distance slowed down the helium-layer erosion process significantly, by a factor of about two. Evolution of vertical density distribution was used to investigate the motion of the helium layer erosion front. The functional dependence of erosion front motion on time was linear in the case of the test with longer jet-obstruction distance. The test with shorter jet-obstruction distance showed a combination of linear and square-root dependence. Transport of gases to an adjacent vessel lead to the creation of a concentration stratification in the adjacent vessel for both of the tests.

The data obtained with high spatial-temporal resolution are currently used for validation of models used in advanced Lumped Parameters codes or Computational Fluid Dynamics codes, which are used for nuclear reactor containment safety analyses.

ACKNOWLEDGMENTS

The authors gratefully acknowledge the support of all the countries participating in the OECD/NEA HYMERES project and the OECD/NEA secretariat. The authors would like to thank all the members of the Management Board and the Programme Review Group of the HYMERES project for their help in defining the test programme and evaluating the test results. The excellent technical support of M. Fehlmann and S. Suter in performing the PANDA HP1 tests is gratefully appreciated.

REFERENCES

1. B. Smith, "Identification and prioritization of generic nuclear safety problems requiring CFD analysis," *Proc. of 17th International Conference on Nuclear Engineering (ICONE17)*, Brussels, Belgium, July 12-16 (2009).
2. B. Schwinges, C. Journeau, T. Haste, L. Meyer, W. Tromm and K. Trambauer, "Ranking of severe accident research priorities," *Progress in Nuclear Energy*, **52**, pp. 11-18 (2010).
3. G. Yadigaroglu, M. Andreani, J. Dreier and P. Coddington, "Trends and needs in experimentation and numerical simulation for LWR safety," *Nuclear Engineering and Design*, **221**, pp. 205-223 (2003).
4. D. Paladino, M. Andreani, R. Zboray and J. Dreier, "Toward a CFD-grade database addressing LWR containment phenomena," *Nuclear Engineering and Design*, **253**, pp. 331-342 (2012).
5. "Investigations of key issues for the simulation of thermal-hydraulics conditions in water reactor containment", OECD/SETH-2 Project, Final Summary report submitted to CSNI, 3 November 2011
6. D. Paladino, S. Guentay, M. Andreani, I. Tkatschenko, J. Brinster, F. Dabbene, S. Kelm, H-J Allelein, D. C. Visser, S. Benz, T. Jordan, Z. Liang, E. Porcheron, J. Malet, A. Bentaib, A. Kiselev, T. Yudina, A. Filippov, A. Khizbullin, M. Kamnev, A. Zaytsev and A. Loukianov, "The EURATOM-ROSATOM ERCOSAM-SAMARA Projects on Containment Thermal-hydraulics of current and future LWRs for Severe Accident Management," *Proceedings of International Congress on Advances in Nuclear Power Plants (ICAPP 2012)*, Chicago, USA, June 24-28, Paper 12325 (2012).
7. D. Paladino, G. Mignot, R. Kapulla, S. Paranjape, M. Andreani, E. Studer, J. Brinster and F. Dabbene, "OECD/NEA HYMERES Project: For the Analysis and Mitigation of a Severe Accident Leading to Hydrogen Release Into a Nuclear Plant Containment," *Proceedings of ICAPP 2014*, Charlotte, USA, April 6-9, Paper 14322 (2014).
8. D. Paladino and J. Dreier, "PANDA a Multi Purposes Integral Test Facility", *Science and Technology of Nuclear Installations*, **2012**, Article ID 239319, doi:10.1155/2012/239319 (2012).
9. R. Zboray, D. Paladino, G. Mignot, N. Erkan, R. Kapulla, M. Ritterath, M. Fehlmann and C. Wellauer, "OECD/NEA SETH-2 Horizontal Fluid Release Tests Test Series Report," *Paul Scherrer Institut, Report TM-42-10-05* (2010).
10. R. Kapulla, S. Kelm, G. Mignot, S. Paranjape and D. Paladino, "Experimental and numerical results for the erosion dynamics of a vertical helium-air jet interacting with a helium-rich layer," *Proceedings of International Congress on Advances in Nuclear Power Plants (ICAPP 2015)*, Nice, France, May 3-6 (2015)
11. R. Kapulla, G. Mignot, S. Paranjape, L. Ryan and D. Paladino, "Large Scale Gas Stratification Erosion by a Vertical Helium-Air Jet," *Science and Technology of Nuclear Installations*, **2014**, Article ID 197267, doi:10.1155/2014/197267 (2014).